Viser Technology Pte. Ltd.
Research and Application of Materials Science
DOI: 10.33142/rams.v3i2.6733

Research Article Open Access

Role of Heat Treatment Temperatures on Mechanical Properties and Corrosion Resistance Properties of Mg-10.16Li-8.14Al-1.46Er alloy

Shuhao LIU, Xiaoyang QIAN, Yun ZOU*

School of Mechanical and Power Engineering, Zhengzhou University, Zhengzhou, China

***Corresponding Author:** *Yun ZOU, No. 100, Science Avenue, High-tech Zone, Zhengzhou City, Henan Province, Zhengzhou 450001, China; yunzou@zzu.edu.cn*

Abstract:
The microstructure and phase evolution of Mg-10.16Li-8.14Al-1.46Er alloy of as-cast, 250℃+12 h, 300℃+12 h, and 400℃+12 h were studied by optical microscopy, scanning electron microscope, and X-ray diffraction. The mechanical properties of Mg-10.16Li-8.14Al-1.46Er alloy in different states were tested by microhardness tester and tension tester. The corrosion resistance of Mg-10.16Li-8.14Al-1.46Er alloy in different states was measured by electrochemical workstation combined with hydrogen evolution and mass loss tests. The results show that the microstructure of as-cast Mg-10.16Li-8.14Al-1.46Er alloy consists of α, β, AlLi, Al_3Er and $MgAlLi_2$ phases. Changes of microstructure are morphology and quantity of α phase, and second phases of $MgAlLi_2$ and AlLi by heat treatments at different temperatures. The best comprehensive tensile properties of Mg-10.16Li-8.14Al-1.46Er at 400℃ are attributed to the α phase structure, solution strengthening and second phase strengthening. After heat treatments at different temperatures, the corrosion resistance of Mg-10.16Li-8.14Al-1.46Er was improved compared with as-cast samples. The Mg-10.16Li-8.14Al-1.46Er alloy has the best corrosion resistance at 250℃ due to the best homogenization at this temperature.
Keywords: *Ultralight Mg-Li alloy; Microstructure; Heat treatments; Mechanical properties; Corrosion resistance properties*

1 Introduction

In the 21st century, with the energy crisis and the environmental crisis, energy conservation and emission reduction have become the universally recognized way of development. Lightweight has become one of the main development ways of energy conservation and emission reduction. It is essential to refer to the lightweight of materials. Mg alloys are the lightest of all structural metals ($\rho \sim 1.74$ g cm^{-2}). Adding lithium (Li) to magnesium (Mg) can form ultralight Mg-Li alloy to further reduce the density of Mg alloys [1-3]. Meanwhile, the problem of difficult deformation of Mg alloys is solved, so Mg-Li alloys are widely used in 3C, medical treatment, automotive electronics and aerospace [4-5]. However, poor corrosion resistance and low strength are still the main problems hindering its large-scale application [6-9]. It is urgent to improve the mechanical and corrosion resistance properties of Mg-Li alloys.

Microstructure determines the properties of materials. To improve the properties of Mg-Li alloy, the most basic is to design the alloy from the angle of alloy casting, so as to obtain the desired microstructure composition. Therefore alloying is a traditional method used to improve the properties of Mg-Li alloy. The addition of Al in Mg-Li alloy can improve the strength of Mg-Li alloy through solution strengthening and dispersion strengthening [10-11]. As for its influence on corrosion resistance, it is reported that the addition of Al will reduce the polarization resistance of Mg-Li alloy, which is detrimental to the corrosion resistance [10]. However, our previous study found that the alloying element Al formed in the Mg-Li alloy presents a refined distribution AlLi phase, which is beneficial to the corrosion resistance of Mg-9Li-6Al alloy [12]. Rare earth elements can significantly improve the strength of Mg-Li alloy through solid solution strengthening and second phase strengthening of forming intermetallic compounds [13-16]. The addition of rare earth element Er can effectively reduce grain size, and appropriate rare earth element Er content makes Mg-10Li-5Zn-0.5Er alloy exhibit the best mechanical properties [17].

Alloying endows the material with a set structure and composition. On the basis of alloying, appropriate heat treatment is applied to adjust the grain size and phase structure and distribution, which can significantly affect

Received on October 2, 2021; Accepted on December 19, 2021

its mechanical and corrosion resistance [18-21]. This is also an important reason why heat treatment is applied in the field of various metal materials. On the other hand, the deformation process of Mg-Li alloy is one of the main strategies applied to improve the performance of Mg-Li alloy [22]. Due to the difficulty of Mg alloys deformation, large deformation will lead to the cracking and micro-cracking of Mg alloy after processing, and seriously affect its service life. Therefore, before the deformation strengthening of Mg-Li alloy, proper heat treatment of the as-cast Mg-Li alloy is needed to improve its machining properties by homogenizing the structure composition, so as to effectively carry out deformation strengthening. Different heat temperatures have different effects on heating treatments. So it is necessary to study the properties and mechanism of properties change of Mg-Li alloy caused by different heat temperatures.

In this paper, as-cast Mg-10.16Li-8.14Al-1.46Er alloy is taken as the research object. For controlling the same heating time, the effects of different heating temperatures on the microstructure, mechanical properties and corrosion resistance properties of Mg-Li alloy are studied. On the one hand, it is expected to improve the properties of Mg-Li alloy through different heating temperatures. On the other hand, it is expected to be a reference for the selection of homogenizing heat treatment temperature of Mg-Li alloy before deformation processing.

2 Material and Methods

2.1 Specimen preparation

The cast Mg-10.16Li-8.14Al-1.46Er ingots were fabricated at the Zhengzhou Light Metals Research Institute of Aluminum Corporation of China Limited (Henan, China). In order to avoid the risk of oxidation at high temperature, the samples were wrapped in tinfoil paper. The heating temperatures were set at 250℃, 300℃, and 400℃, and the heating time was set as 12 h. Water quenching was carried out immediately after the heat treatment.

2.2 Material characterization

2.2.1 Microstructure characterization

After mechanical polishing and washing, samples were etched using a 4 vol.% nitric acid alcohol solution. Then, the microstructure was observed by VHX-2000 optical microscopy (OM) (Keyence, Osaka, Japan) or an Auriga-bu scanning electron microscopy (SEM) (Zeiss, Jena, GER) with the acceleration voltage of 5 kV. The phase evolution was analyzed by Empyrean X-ray diffraction (XRD) technology (Malvenpanako, NL, USA). The voltage and current were 45 kV and 40 mA, respectively. The diffraction angle (2θ) ranged from 20° to 80 °.

2.2.2 Mechanical properties characterization

The hardness test force of samples in different heat treatment states is 0.5 N, and the load time is maintained for 10 s by HV-1000 Vickers microhardness tester (Beijing Times Mountain Peak Technology, Beijing, CN) with the size of samples was 10×10×2 mm. The tensile test was carried out on a MTS370.25 tension tester (MTS Systems Corporation, Minnesota, USA) with a displacement rate of 1.5 mm/min. The gauge length, width, and thickness of the tensile specimens were 25, 10 and 2 mm, respectively.

2.2.3 Corrosion resistance characterization

The corrosion resistance of the samples was characterized by polarization curve test, hydrogen evolution test and mass loss test. The polarization curve test was tested using an RST5200F electrochemical workstation (Zhengzhou SRIS Instrument Technology, Zhengzhou, CN), in which the working electrode was the test samples, the platinum plate was the counter electrode, and the saturated calomel electrode was the reference electrode. The samples were immersed in 3.5 wt. % NaCl solution with an exposure area of 1 cm^2. The polarization measurements started from −0.15 V to 0.15 V (relative to the open circuit potential) with a scanning rate of 0.5 mV/s. In order to directly compare the corrosion rate measured by electrochemical test with hydrogen evolution test and mass loss test, the results were characterized by annual corrosion rate.

The corrosion current density i_{corr} (mA cm^{-2}) is related to the corrosion rate P_i (mm y^{-1}) and the conversion equation [18,23,24]:

$$P_i = 22.85i_{corr} \quad (1)$$

For hydrogen evolution test, the samples were immersed in 3.5wt. % NaCl solution (exposure area was 2 cm^2) for 72 h. The mass W_1 of the sample was recorded before the test, and the volume change was recorded every hour during the test. After the immersing, the samples were immersed in 180 g/L CrO_3 solution for 5 min and cleaned by ultrasound. Weigh and record W_2 after removing corrosion products. The hydrogen evolution volume rate V_H (mm cm^{-2} d^{-1}) was converted to corrosion rate P_H (mm y^{-1}), and the conversion equation was obtained [18,23,24]:

$$P_H = 2.279V_H \quad (2)$$

Mass loss rate $\triangle W_m$ (mg cm^{-2} d^{-1}) is converted to corrosion rate P_W (mm y^{-1}), the conversion equation [18,23,24]:

$$P_W = 2.10\Delta W_m \quad (3)$$

3 Results

3.1 Microstructure

The microstructures of Mg-10.16Li-8.14Al-1.46Er before and after different heat treatments were shown in Figure 1. The microstructures of all samples were characterised by the α phase, β matrix phase and black second phase particles, which the composition of the main phases does not change.However, it is observed that

the α phase changes to a smaller and elongated direction at 250℃ compared with the as-cast sample. Changes of α phase are more obvious at 300℃, and the distribution of α phase is fine at grain boundaries (GBs). The second black phase particles are decreased obviously. When heating temperatures at 400 ℃, the microstructure changes particularly obvious as showed in Figure 1d. The α phase distributed at the GBs shows a trend of spheroidization increasing along the GBs, while the number of α phase decreases. Then the α phase on the β phase matrix shows a relatively fine distribution. The second black phase particles are basically disappeared.

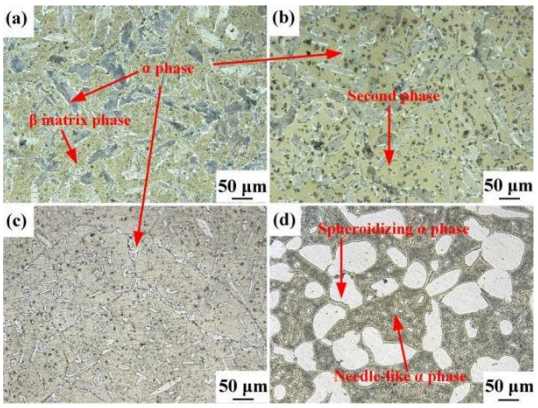

Figure 1 The microstructure of Mg-10.16Li-8.14Al-1.46Er alloy (a) As-cast, (b) 250℃, (c) 300℃, and (d) 400℃

Figure 2 shows the XRD patterns of Mg-10.16Li-8.14Al-1.46Er alloy before and after different heat treatments. The diffraction peaks of as-cast Mg-10.16Li-8.14Al-1.46Er alloy includes α phase, β phase, AlLi phase, Al_3Er and $MgAlLi_2$ phase. When the heating temperature is 250℃, the composition of the main phase does not change, but the diffraction peaks of the $MgAlLi_2$ phase almost disappear, which is consistent with the results of microstructure. However, diffraction peaks of $MgAlLi_2$ phase were reappeared again at 300℃, and the intensity of $MgAlLi_2$ phase diffraction peak increases at 400℃, the diffraction peaks of AlLi phase were disappeared. In other words, the changes of Mg-10.16Li-8.14Al-1.46Er alloy after different heat treatments were mainly the second phases.

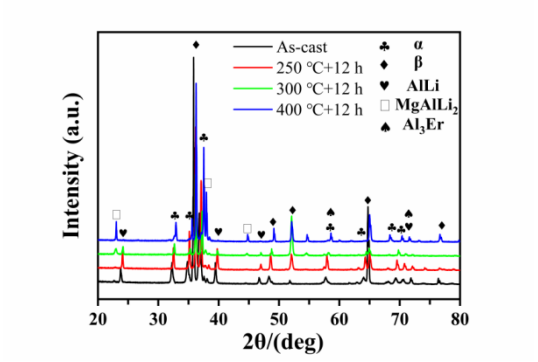

Figure 2 XRD patterns of Mg-10.16Li-8.14Al-1.46Er alloy

3.2 Mechanical properties

3.2.2 Microhardness

The hardness of Mg-10.16Li-8.14Al-1.46Er alloy before and after different heat treatments was shown in Figure 3. The hardness of Mg-10.16Li-8.14Al-1.46Er alloy was increased by different heat treatments and the changes of hardness value were attributed to microstructure. Combined with the analysis of microstructure and XRD patterns, the $MgAlLi_2$ phase disappears at 250℃, while the $MgAlLi_2$ phase is a metastable precipitation phase, which is easy to decompose and produce AlLi phase, thus resulting in softening effect [25-26]. However, the hardness value increased significantly at 250℃, and the peak strength of AlLi at 250℃ did not increase, which indicating that part of AlLi phases were solidly dissolved into the matrix, thus producing a solid solution strengthening effect. The hardness value of samples at 300℃ was 15% higher than as-cast samples. However, hardness value of 300℃ was lower than hardness value of 250℃. This is likely due to the refinement of α phase, which increases the proportion of the softer β matrix phase, resulting in a decrease in hardness. XRD patterns show that $MgAlLi_2$ phase is precipitated again, diffraction intensity of AlLi phase decreased. Therefore, the strengthening effect was attributed to precipitation strengthening and solid solution strengthening. The hardness of samples at 400℃ was 23.8% higher than as-cast samples. In this condition, the diffraction peak intensity of $MgAlLi_2$ phase was further enhanced and the diffraction peaks of AlLi phases disappear, which means that stronger precipitation strengthening and solid solution strengthening occur at this temperature. Therefore, the hardness values increases remarkably.

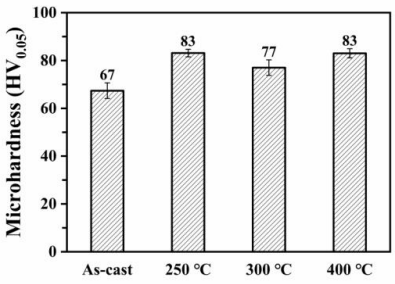

Figure 3 Microhardness of the Mg-10.16Li-8.14Al-1.46Er alloy

3.2.2 Tensile properties

Figure 4 is the engineering stress-strain curves of the Mg-10.16Li-8.14Al-1.46Er alloy before and after different heat treatments, and the tensile mechanical related parameters are summarized in Table 1. The tensile strength (UTS) of Mg-10.16Li-8.14Al-1.46Er alloy of as-cast, 250℃, 300℃ and 400℃ was 180, 221, 237 and 226 MPa, respectively. The yield strength (YTS) was 151, 180, 225 and 198 MPa, respectively. The fracture elongation (E_f) was 3.0, 3.1, 1.4 and 4.8%, respectively. The UTS of Mg-10.16Li-8.14Al-1.46Er alloy at 250℃

was 22.8% higher than as-cast samples. However, the E_f does not change significantly compared to the strength. The UTS of Mg-10.16Li-8.14Al-1.46Er alloy at 300℃ was 31.7 % higher than as-cast samples, but the plastic loss is serious. The UTS of samples at 400℃ was 25.6% higher than as-cast samples and the E_f was highest.

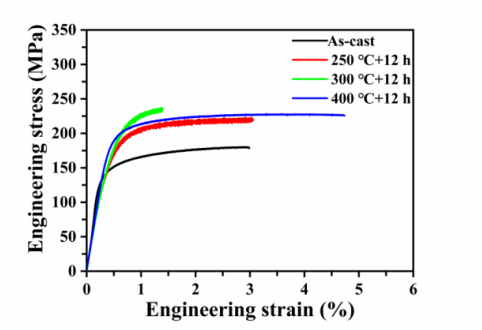

Figure 4 Engineering stress-strain curve of Mg-10.16Li-8.14Al-1.46Er alloy

Table 1 Tensile mechanical properties of Mg-10.16Li-8.14Al-1.46Er alloy

Sample	As-cast	250℃	300℃	400℃
TYS (MPa)	151	180	225	198
UTS (MPa)	180	221	237	226
E_f (%)	3.0	3.1	1.4	4.8

3.3 Corrosion resistance

Figure 5 is the polarization curves of Mg-10.16Li-8.14Al-1.46Er alloy. The corrosion potentials of samples of as-cast, 250℃, 300℃ and 400℃ were − 1.61 V, − 1.62 V, − 1.58 V and − 1.57V, respectively as showing in Figure 5b. The corrosion potential reflects the corrosion tendency of samples, which the more negative of the corrosion potential, the greater of the corrosion tendency. According to the corrosion potential value, the samples at 300℃ had the smallest corrosion tendency. However, the corrosion tendency represented by corrosion potential has no relation with the actual corrosion rate, and the corrosion current density determines the corrosion rate of the samples. The corrosion current density of Mg-10.16Li-8.14Al-1.46Er alloy of as-cast, 250℃, 300℃ and 400℃ was 1.25×10^{-1}, 1.19×10^{-1}, 0.79×10^{-1} and 0.6×10^{-1} mA • cm^{-2}, respectively. Then the order of corrosion rates from low to high was: 400℃＜300℃＜250 ℃＜ as cast. This means that the corrosion resistance of as-cast Mg-10.16Li-8.14Al-1.46Er alloy was improved by different heat treatments.

According to the corrosion current density value substituted into formula (1) for calculation, the corrosion rate P_i (mm y^{-1}) of Mg-10.16Li-8.14Al-1.46Er alloy in different states was 2.86, 2.72, 1.80 and 1.37 mm y^{-1}, respectively. The corrosion current density measured by the polarization curve reflects the transient measurement. The actual corrosion rates of different Mg-Li alloys need to analyze in combination with long-term immersion corrosion tests.

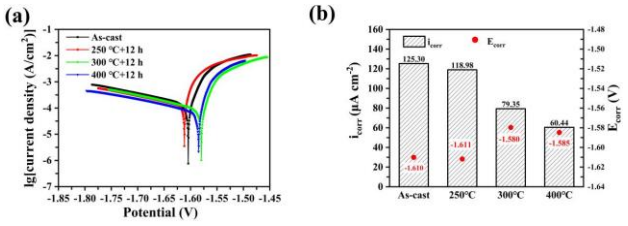

Figure 5 Polarization curves of the Mg-10.16Li-8.14Al-1.46Er alloy (a) and corrosion potential and current density (b)

Figure 6 is the immersion test results of Mg-10.16Li-8.14Al-1.46Er alloy. It can be seen from Figure 6a that the volume of hydrogen evolution of as-cast and at 300℃ samples was significantly higher than the other two heat treatment status samples at the initial stage. The hydrogen evolution of the samples at 400℃ was always lower until the immersion time of 45 h. The volume of hydrogen evolution of samples at 400℃ exceeds the samples at 250℃ after 45 h, then exceeds the samples at 300℃ after 63 h. The final volume of hydrogen evolution was as follows: as cast ＞ 400 ℃ ＞ 300℃ ＞ 250℃. This means that the corrosion resistance of the samples immersed in 3.5 wt. % NaCl solution for a long time after heat treatment at 400℃ was only higher than the as-cast alloy. The hydrogen evolution rate V_H (mm cm^{-2} d^{-1}) of Mg-10.16Li-8.14Al-1.46Er of as-cast, 250℃, 300℃ and 400 ℃ was 8.70, 4.35, 4.95 and 5.56 mm cm^{-2} d^{-1}, respectively. According to formula (2), the V_H converted to corrosion rate P_H (mm y^{-1}) and the hydrogen evolution corrosion rate was: 19.83, 9.91, 11.28 and 12.67 mm y^{-1}, respectively.

Figure 6b is the mass loss of Mg-10.16Li-8.14Al-1.46Er alloy. The mass loss of samples of as-cast, 250℃, 300℃ and 400℃ was 9.8, 3.5, 4.9 and 5.8 mg cm^{-2} d^{-1}, respectively. The corrosion rate of samples was as follows: as-cast ＞ 400℃ ＞ 300℃ ＞ 250 ℃. The results of hydrogen evolution test consistent with the results of mass loss test. According to formula (3), the corrosion rates P_W (mm y^{-1}) was 20.85, 7.35, 10.29 and 12.18 mm y^{-1}, respectively.

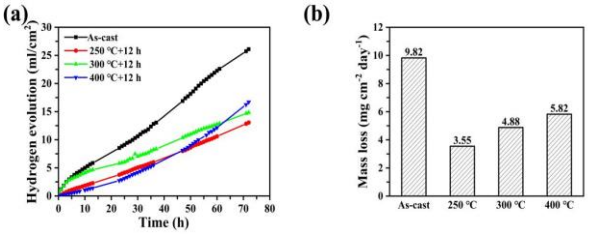

Figure 6 Hydrogen evolution curves (a) and mass loss (b) of the Mg-10.16Li-8.14Al-1.46Er alloy immersed in 3.5 wt. % NaCl solution for 72 h.

4 Discussion

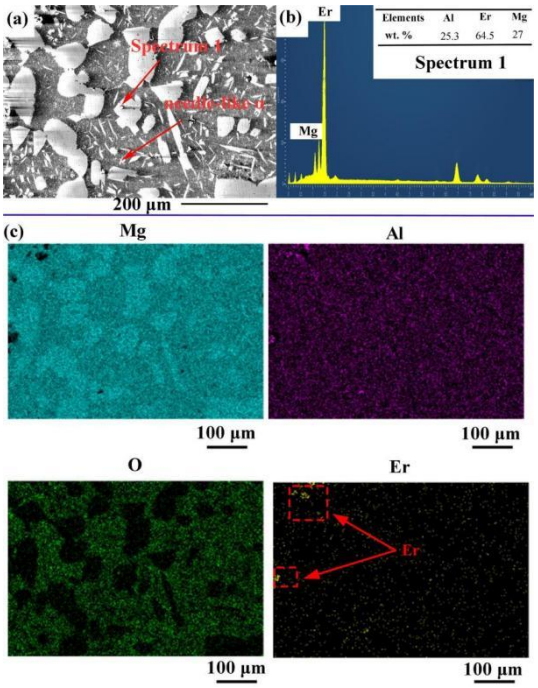

Figure 7 SEM and EDS of Mg-10.16Li-8.14Al-1.46Er alloy by heat treatment at 400℃. (a) microstructure. (b) point scan map. (c) surface scan map

The properties of the alloys are determined by the microstructure. Through the analysis of the observation results in Figure 1, the main phase of α was not obviously changed by heat treatment at the relatively lower temperature. This is due to there was no supersaturated solid solution formation, while no phase was precipitated during the water quenching. With the increase of temperature for 300℃, according to XRD analysis in Figure 2, AlLi phase was the main phase that disappeared and the $MgAlLi_2$ phase diffraction peak appears. $MgAlLi_2$ phase is a metastable phase and it is decomposed at 250℃, part of which is dissolved into α phase, and the other part is transformed into AlLi phase. With the increase of temperature to 300℃, supersaturated solid solution will be formed and $MgAlLi_2$ will precipitate again during water cooling. At 400℃, the diffraction peak of $MgAlLi_2$ phase is further strengthened. Moreover the α phase decreases obviously, while the α phase at GBs becomes larger than the α phase in matrix at 300℃. In order to further analyze the morphology distribution and elemental composition of α phase at 400℃, the SEM and energy spectrum analysis (EDS) was used to observe the microstructure at this temperature, and the results were shown in Figure 7. It can be seen from Figure 7a that bright white particles were distributed in the α phase, which is Al_3Er phase by point scanning element analysis in Figure 7b. This is further confirmed by the plane sweep diagram in Figure 7c, which the Er element was distributed on the α phase. The results show that the supersaturated solid solution was formed at higher temperature. During water quenching, part of α phases precipitates from the matrix phase and presents a fine needle-like distribution [27]. However, abnormal growth of α phase at the GBs may be related to the heterogeneous nucleation (such as Al_3Er). Changes of α phase and second phase caused by different heat treatments will result in different mechanical properties and corrosion resistance properties.

4.1 Analysis of tensile properties

The tensile properties of Mg-10.16Li-8.14Al-1.46Er alloy by different heat treatments were obviously different. Figure 8 is the SEM of tensile fractures of Mg-10.16Li-8.14Al-1.46Er alloy before and after different heat treatments. It can be seen on the fracture surface of Mg-10.16Li-8.14Al-1.46Er alloy in different states was not only composed of dimples, and there are still many cleavage planes on the surface. According to the tensile test results, the heat treatment temperature of 300℃ has the highest strength and the worst plasticity. It can be seen from Figure 8b and c that the dimples on the fracture surfaces of Mg-10.16Li-8.14Al-1.46Er alloy at 250℃ and 300℃ are small and shallow, but the cleavage plane of a hexagon appears on the surface of Mg-10.16Li-8.14Al-1.46Er alloy at 300℃, indicating that a poor plasticity. According to XRD results, strengthening phase of $MgAlLi_2$ appears in this state, and softened phase of AlLi is partially solute, which is also a reason for its plasticity deterioration. At the same time, bright white inclusions were found on the fracture surface of Mg-10.16Li-8.14Al-1.46Er alloy at 400℃ in Figure 8d. EDS results show that the atomic ratio of Er element to Al element is about 2.7. It means that bright white inclusion was Al_3Er phase. The above tensile test results show that the strength of Mg-10.16Li-8.14Al-1.46Er alloy at 400℃ was relatively higher, which the higher strength may be related to solid solution strengthening and second phase strengthening. Figure 9 is the optical microstructure of the fracture surface of Mg-10.16Li-8.14Al-1.46Er alloy before and after different heat treatments. The tensile test results show that Mg-10.16Li-8.14Al-1.46Er alloy at 400℃ has higher strength and the best plasticity, while the Mg-10.16Li-8.14Al-1.46Er alloy at 300 ℃ has the highest strength. According to the observation of microstructure on the fracture surface, there were bigger spheroidizing α phases distributed along the fracture surface in Figure 9d. As for duplex phases Mg-Li alloy, α phase can coordinate strength and β phase coordinate plastic. So the distribution of fewer but larger α phases increased the strength, and more β phases proportion improved the plasticity. However, the surface of the fracture shows a tearing zigzag shape at 300℃ in Figure 9c, which indicates that the fracture was sudden. The fracture plane passes through the α phase, and part of the α phases was torn. These torn α phases were rod-shaped, which contributing strong but decreasing plasticity. Morphology and distribution of α phase and the formation

of intermetallic compounds are important factors affecting the mechanical properties of samples.

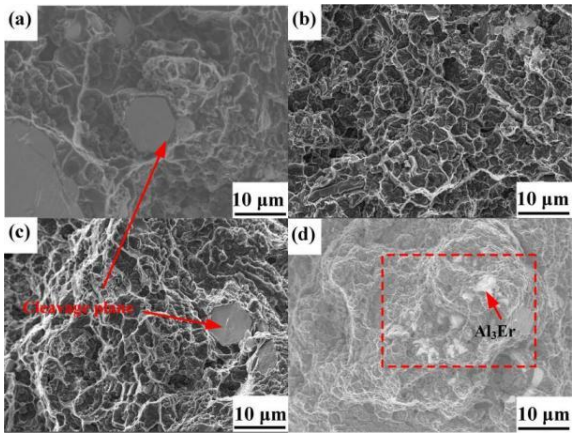

Figure 8 SEM of fracture surface of Mg-10.16Li-8.14Al-1.46Er alloy. (a) as-cast. (b) 250℃. (c) 300℃. (d) 400℃

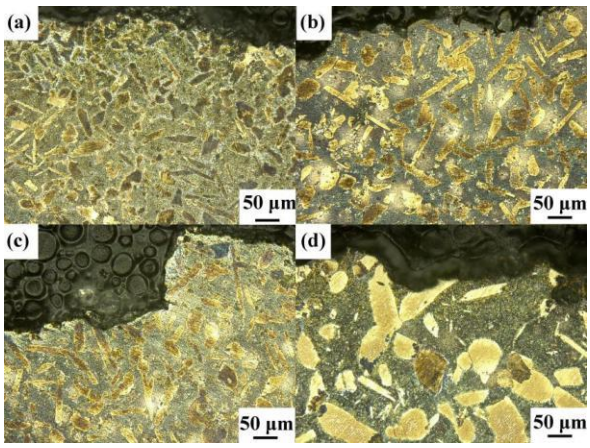

Figure 9 Optical microstructures of fracture surface of Mg-10.16Li-8.14Al-1.46Er alloy. (a) as-cast. (b) 250℃. (c) 300℃. (d) 400℃

4.2 Analysis of corrosion resistance properties

The results of three kinds of corrosion resistance tests show that the corrosion resistance of Mg-10.16Li-8.14Al-1.46Er alloy after heat treatments was improved compared with as-cast alloys. While the corrosion resistance of Mg-10.16Li-8.14Al-1.46Er alloy by different heat treatments was different. On the one hand, it is related to the type of corrosion products, on the other hand, it is related to the phase structure of Mg-Li alloy. Figure 10 is the surface morphology of Mg-10.16Li-8.14Al-1.46Er alloy before and after different heat treatments immersed in 3.5 wt. % NaCl solution for 72 h. According to the macroscopic corrosion morphology of Figure 10a,c,e,g, the corrosion surface of Mg-10.16Li-8.14Al-1.46Er alloy was distributed at corrosion pits. From microscopic corrosion morphology of Figure b,d,f,h, the corrosion not only corroded the β phase, but also corroded the α phase in a large area. The results show that pitting corrosion is the main corrosion type of different samples. This indicates that samples in different states have experienced serious corrosion during immersion. For Mg-Li alloy, the main protective film components are Li_2CO_3 and $MgCO_3$. However, with the progress of immersion test, corrosion occurs preferentially in the β phase, and the corrosion products are mainly $Mg(OH)_2$ and LiOH, which are porous and not protective, unable to resist the erosion of Cl^-. As corrosion progresses, the α phase is corroded. But compared with as-cast Mg-10.16Li-8.14Al-1.46Er alloy, heat treatment improves the corrosion resistance of Mg-10.16Li-8.14Al-1.46Er alloy. Figure 11 is the corrosion section morphology along the depth direction of Mg-10.16Li-8.14Al-1.46Er alloy before and after different heat treatments. Mg-10.16Li-8.14Al-1.46Er alloy is mainly composed of α and β phases, which is consistent with the microstructure analysis. The top of the section morphology is uneven in Figure 11a,c,d, which corrosion occurs on the surface and gradually corroded in the direction of depth after a long time immersion. According to Figure 1 and 2, the microstructure changes of Mg-10.16Li-8.14Al-1.46Er alloy at 300℃ lies in the refinement of α phase, $MgAlLi_2$ phase and AlLi phase. The refinement of α phase exposes more β phases to immersion corrosion medium, resulting in the outstanding hydrogen evolution of in the early stage of hydrogen evolution as showed in Figure 11c. Uniform corrosion in Figure 11b proves that the samples at 250℃ have the best corrosion resistance from the long time immersion. It can be seen from Figure 6a that the hydrogen evolution range of Mg-10.16Li-8.14Al-1.46Er alloy at 250 ℃ shows a relatively consistent linear change with time, which means that it has a good homogenization effect. While the polarization curve test combined with the preliminary analysis of hydrogen evolution test shows the best corrosion resistance in a short time at 400℃. At the same time, it is also found that no matter what the state of samples is, it preferentially corrodes the β phase when the corrosion occurs. With corrosion of β phase leads to falling off α phase. The best corrosion resistance in a short time at 400℃ due to inhibitory effect of α phase. The microstructure changes of Mg-10.16Li-8.14Al-1.46Er alloy at 400℃ not only on α phase but also the second phases. That is AlLi phase was solidly dissolved into the matrix and precipitation $MgAlLi_2$ phase. Immersing in the early stage of the samples at 400℃, corrosion resistant performance was outstanding due to the distribution of spheroidizing α phase and needle-like α phase. However, with the process of immersion, corrosion takes place preferentially in β phase. At the same time, AlLi phase distributed in α/β phase boundary plays the role of corrosion barrier [12-28]. But AlLi phase was solidly dissolved after heat treatment at 400℃, which means that its barrier effect disappears. Therefore, the β phase matrix corrosion is serious with the progress of corrosion, while the α phase loses protection. Then the volume of hydrogen evolution was increasing.

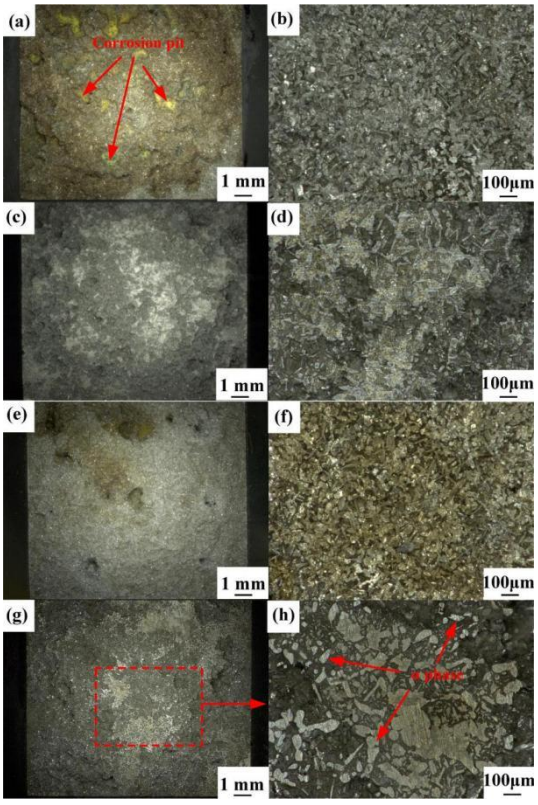

Figure 10 Surface morphology of Mg-10.16Li-8.14Al-1.46Er alloy immersed in 3.5 wt. % NaCl solution for 72 h. (a, b) as-cast. (b, c) 250℃. (e, f) 300℃. (g, h) 400℃

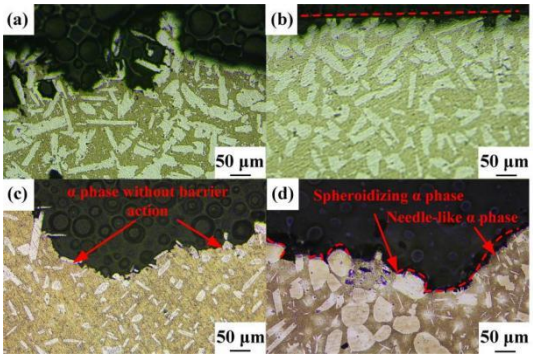

Figure 11 Section morphology of Mg-10.16Li-8.14Al-1.46Er alloy immersed in 3.5 wt. % NaCl solution for 72 h. (a) as-cast. (b) 250℃. (c) 300℃. (d) 400℃

5 Conclusions

The comprehensive mechanical and corrosion properties of Mg-10.16Li-8.14Al-1.46Er were investigated before and after heat treatments. The main conclusions are summarized as following:

(1) The microstructure of as-cast Mg-10.16Li-8.14Al-1.46Er includes α, β, $MgAlLi_2$, Al_3Er and AlLi. After heat treatments at different temperatures, the microstructure changes are the morphology and quantity of α phase, the second phases of $MgAlLi_2$ and AlLi.

(2) After heat treatments at different temperatures, the hardness and strength of Mg-10.16Li-8.14Al-1.46Er alloy were improved compared with the as-cast samples. At 400℃, Mg-10.16Li-8.14Al-1.46Er alloy has the best comprehensive mechanical properties due to its α phase structure, solution strengthening and second phase strengthening.

(3) After heat treatments at different temperatures, the corrosion resistance of Mg-10.16Li-8.14Al-1.46Er was improved compared with the as-cast samples. The Mg-10.16Li-8.14Al-1.46Er alloy has the best corrosion resistance at 250℃ due to the best homogenization at this temperature.

Author Contributions: Shuhao Liu: Investigation, Methodology, Data curation, Validation, Writing – original draft preparation. Xiaoyang Qian: Methodology, Validation, Visualization. Yun Zou: Methodology, Validation, Writing – review & editing, Supervision, Funding acquisition. All authors have read and agreed to the published version of the manuscript.

Conflict of Interest: The authors declare that there is no conflict of interest regarding the publication of this paper.

Acknowledgments: This research was funded by the National Natural Science Foundation of China (No. 51801185); Key Research Project of the Higher Education Institutions of Henan Province, Henan Provincial Department of Education, China (No. 19A460007); and Training Program for Young Backbone Teachers of the Higher Education Institutions of Henan Province, China. The authors would like to thank the experimental equipment support by Center of Advanced Analysis & Gene Sequencing, Zhengzhou University, China.

References

[1] Xu W Q, Birbilis N. A high-specific-strength and corrosion-resistant magnesium alloy. Nature 2015, 14: 1229–1235.

[2] Zhao J, Zhang J. Effect of Y content on microstructure and mechanical properties of as-cast Mg-8Li-3Al-2Zn alloy with duplex structure. Mater. Sci. Eng. A 2016, 650: 240–247.

[3] Mineta T, Sato H. Simultaneously improved mechanical properties and corrosion resistance of Mg-Li-Al alloy produced by severe plastic deformation. Mater. Sci. Eng. A 2018, 735: 418–422.

[4] Liu T, Yang Q. Stability of twins in Mg alloys – A short review. J. Magnes. Alloy. 2020, 8: 66–77.

[5] Pu Z, Yang S. Ultrafine-grained surface layer on Mg-Al-Zn alloy produced by cryogenic burnishing for enhanced corrosion resistance. Scr. Mater. 2011, 65: 520–523.

[6] Li R G, Li H R. Achieving exceptionally high strength in binary Mg-13Gd alloy by strong texture and substantial precipitates. Scr. Mater. 2021, 193: 142–146.

[7] Pugazhendhi B S, Kar A. Effect of aluminium on microstructure, mechanical property and texture evolution of dual phase Mg-8Li alloy in different processing conditions. Arch. Civ. Mech. Eng. 2018, 18: 1332–1344.

[8] He Y, Peng C. Effects of alloying elements on the microstructure and corrosion behavior of Mg-Li-Al-Y alloys. J. Alloys Compd. 2020, 834.
[9] Sun Y H, Wang R C. Corrosion behavior and surface treatment of superlight Mg-Li alloys. T. Nonferr. Metal. Soc. 2017, 27: 1455–1475.
[10] Guo J, Chang L L. Effect of Sn and Y addition on the microstructural evolution and mechanical properties of hot-extruded Mg-9Li-3Al alloy. Mater. Charact. 2019, 148: 35–42.
[11] Morishige T, Obata Y. Effect of Al composition on the corrosion resistance of Mg-14 mass% Li system alloy. Mater. Trans. 2016, 57: 1853–1856.
[12] Zou Y, Zhang L. Improvement of mechanical behaviors of a superlight Mg-Li base alloy by duplex phases and fine precipitates. J. Alloys Compd. 2018, 735: 2625–2633.
[13] Cao D, Wu L. Electrochemical behavior of Mg-Li, Mg-Li-Al and Mg-Li-Al-Ce in sodium chloride solution. J. Power Sources 2008, 177: 624–630.
[14] Sun Y, Wang R. Microstructure and corrosion behavior of as-extruded Mg-xLi-3Al-2Zn-0.2Zr alloys (x = 5, 8, 11 wt.%). Corros. Sci. 2020, 167.
[15] Sun Y, Wang R. Hot deformation behavior of Mg-8Li-3Al-2Zn-0.2Zr alloy based on constitutive analysis, dynamic recrystallization kinetics, and processing map. Mech. Mater. 2019, 131: 158–168.
[16] Cao F, Zhang J. Mechanical properties and microstructural evolution in a superlight Mg-6.4Li-3.6Zn-0.37Al-0.36Y alloy processed by multidirectional forging and rolling. Mater. Sci. Eng. A 2019, 760: 377–393.
[17] Ji H, Liu W. Influence of Er addition on microstructure and mechanical properties of as-cast Mg-10Li-5Zn alloy. Mater. Sci. Eng. A 2019, 739: 395–403.
[18] Wang G W, Song D. Developing improved mechanical property and corrosion resistance of Mg-9Li Alloy via solid-solution treatment. Metals 2019, 9.
[19] Li J, An J. Effects of solution heat treatment on the microstructure and hardness of Mg-5Li-3Al-2Zn-2Cu alloy. Mater. Sci. Eng. A 2010, 527: 7138–7142.
[20] Pradeep Kumar P, Raj Bharat A. Role of microstructure and secondary phase on corrosion behavior of heat treated AZ series magnesium alloys. Mater. Today 2019, 18: 175-181.
[21] Maurya R, Mittal D. Effect of heat-treatment on microstructure, mechanical and tribological properties of Mg-Li-Al based alloy. J. Mater. Res. Technol. 2020, 9: 4749–4762.
[22] Wang B, Xu K. Anisotropic corrosion behavior of hot-rolled Mg-8 wt.%Li alloy. J. Mater. Sci. Technol. 2020, 53: 102–111.
[23] Shi Z, Liu M. Measurement of the corrosion rate of magnesium alloys using Tafel extrapolation. Corros. Sci. 2010, 52: 579–588.
[24] Shi Z, Atrens A. An innovative specimen configuration for the study of Mg corrosion. Corros. Sci. 2011, 53: 226–246.
[25] Wu R, Zhang M. Microstructure, mechanical properties and aging behavior of Mg-5Li-3Al-2Zn-xAg. Mater. Sci. Eng. A 2009, 520: 36–39.
[26] Guo X, Wu R. Influences of solid solution parameters on the microstrucuture and hardness of Mg-9Li-6Al and Mg-9Li-6Al-2Y. Mater. Des. 2014, 53: 528-533.
[27] Kral M V, Muddle B C. Crystallography of the bcc/hcp transformation in a Mg-8Li alloy. Mater. Sci. Eng. A 2007, 460–461.
[28] Song G S, Staiger M. Some new characteristics of the strengthening phase in β-phase magnesium-lithium alloys containing aluminum and beryllium. Mater. Sci. Eng. A 2004, 371: 371–376.